



## Optimal elliptical retarder in rotating compensator imaging polarimetry

DALE GOTTLIEB<sup>1</sup> AND ORIOL ARTEAGA<sup>1,2,\*</sup>

<sup>1</sup>Dep. Física Aplicada, Feman Group, Universitat de Barcelona, Barcelona 08028, Spain

<sup>2</sup>Institute of Nanoscience and Nanotechnology (IN2UB), Universitat de Barcelona, Barcelona 08028, Spain

\*Corresponding author: oarteaga@ub.edu

Received 28 April 2021; revised 1 June 2021; accepted 2 June 2021; posted 2 June 2021 (Doc. ID 430266); published 23 June 2021

**In this Letter, we present a new, to the best of our knowledge, design for elliptical retarders based on two quarter-wave retarders with an angle offset, which is particularly well suited for polarimetric measurements based on rotating compensator systems. We show that this simple elliptical retarder design offers the minimum condition number achieved by traditionally optimal polarimeter setups and can be used to further improve the accuracy of polarimetric imaging measurements in the presence of error sources, with the advantage that it only requires common quarter-wave retarders.** © 2021 Optical Society of America

<https://doi.org/10.1364/OL.430266>

Polarimetric analysis, the study of polarized light beams and their interactions with materials, has a large number of applications, ranging from cancer diagnosis to geological studies [1,2]. The most common polarimeter design uses a rotating compensator and a static polarizer to measure the full Stokes vector of the input light [3]. The same design can be used to generate states of polarization for polarimeters measuring the Mueller matrix [4]. Previous studies have shown that rotating compensator devices are optimized when a compensator with an  $\sim 132^\circ$  retardance is used, and rotated to a minimum of four optimal pre-determined angles, although a higher number of measurement angles can achieve a higher error tolerance of the setup [5,6].

However, since most compensators are designed at either quarter- or half-wave retardances, purchasing components for an optimal polarimeter can be a challenge. Custom Fresnel rhombs can be manufactured to work over a broad wavelength range, but these devices have a small entrance pupil, which limits the field of view (FOV) for polarimetric imaging systems [6,7]. Moreover, these custom devices are expensive and have a long lead time required to manufacture them. A polymer film compensator offers a larger FOV at a much lower price than a Fresnel rhomb, but these devices are not achromatic, and they are rarely found at  $132^\circ$  retardance values.

In this Letter, we propose the use of a simple elliptical retarder composed of combinations of two quarter-wave plate (QWP) retarders to create a polarimetric imaging system with complete equivalency to one with a single  $132^\circ$  retarder. Although previous studies have analyzed the use of two QWPs in polarimetric systems [8–12], this work presents a novel approach of using a fixed angle between the two retarders and rotating them as a

couple, removing the need for a second motor to independently rotate the compensators. This allows to effectively consider a single elliptical compensator with constant values of linear and circular retardance, but with a changing azimuth. Moreover, we extend this analysis to a broad range of compensators with retardances ranging over  $\pm 20^\circ$  from a QWP, which has not been addressed in previous studies, to the best of our knowledge.

By adjusting the relative angle between the two compensators, the effective linear birefringence can be tuned, allowing this device to work with optimal performance even when operating at over  $\pm 100$  nm from the designed wavelength of a simple zero-order polymer wave plate. Moreover, since our system is equivalent to one using a single  $132^\circ$  retarder in terms of polarimetric analysis, the optimum angles previously reported for polarimeters for any number of measurements can still be applied to these setups with just a constant offset, and they do not need to be re-calculated at every setting. This work allows for a polarimetric imaging system to be built with a wide FOV and broad wavelength tunability, all while using very inexpensive off-the-shelf components. Furthermore, it can be extended to full Mueller matrix analysis setups.

A full Stokes polarimeter is best described by taking advantage of Stokes–Mueller calculus. Thus, the Stokes vector measured by the system,  $\mathbf{S}_{\text{out}}$ , equals

$$\mathbf{S}_{\text{out}} = \mathbf{P}_1 \mathbf{R}(-\theta) \mathbf{M}_{LR} \mathbf{R}(\theta) \mathbf{S}_{\text{in}}, \quad (1)$$

where  $\mathbf{P}_1$  is the Mueller matrix of a polarizer, and  $\mathbf{R}(\theta)$  and  $\mathbf{M}_{LR}$  are given as

$$\mathbf{R}(\theta) = \begin{pmatrix} 1 & 0 & 0 & 0 \\ 0 & \cos(2\theta) & \sin(2\theta) & 0 \\ 0 & -\sin(2\theta) & \cos(2\theta) & 0 \\ 0 & 0 & 0 & 1 \end{pmatrix} \quad (2)$$

and

$$\mathbf{M}_{LR} = \begin{pmatrix} 1 & 0 & 0 & 0 \\ 0 & 1 & 0 & 0 \\ 0 & 0 & \cos(\delta) & -\sin(\delta) \\ 0 & 0 & \sin(\delta) & \cos(\delta) \end{pmatrix}, \quad (3)$$

where  $\delta$  is the linear retardance of the compensator, and  $\theta$  is the rotation angle that defines the azimuth angle of the compensator.

Since the detector only measures the intensity of light, we consider only the top row of the multiplication, and the measured intensity is therefore given as [5]

$$\begin{aligned} \mathbf{I}_k = & [1, \cos^2(2\theta_k) + \cos(\delta) \sin^2(2\theta_k), \sin^2(\delta/2) \sin(4\theta_k) \\ & - \sin(\delta) \sin(2\theta_k)] \mathbf{S}_{\text{in}} = \mathbf{W}_k \mathbf{S}_{\text{in}}, \end{aligned} \quad (4)$$

where  $\mathbf{I}_k$  is the intensity on the  $k^{\text{th}}$  measurement,  $\theta_k$  is the angle of the compensator, and  $\mathbf{W}$  is termed the measurement matrix, with  $\mathbf{W}_k$  being the  $k^{\text{th}}$  row of  $\mathbf{W}$ . Since we are seeking to solve for the input Stokes vector, we rearrange the equation as

$$\mathbf{S}_{\text{in}} = \mathbf{W}^+ \mathbf{S}_{\text{out}}, \quad (5)$$

where  $\mathbf{W}^+$  is the pseudo-inverse of  $\mathbf{W}$  ( $\mathbf{W}^+ = (\mathbf{W}^T \mathbf{W})^{-1} \mathbf{W}^T$ ), which gives a least-squares estimate of the inverse. This matrix is invertible when the determinant of  $\mathbf{W}^T \mathbf{W}$  is not equal to 0, and the error in the measurement is minimized when the determinant is maximized. Equivalently, the condition number

$$\text{cond}(\mathbf{W}) = \|\mathbf{W}\| \|\mathbf{W}^+\| \quad (6)$$

is minimized to a value of  $\sqrt{3}$  in an optimal system [13,14].  $\|\dots\|$  denotes here the matrix norm, which, in the context of polarimetry, is usually chosen as the 2-norm. Through numerical optimization techniques, it has been previously shown that the ideal settings for  $N=4$  measurements is when  $\delta$  is  $132^\circ$  and  $\theta$  is  $\pm 51.7^\circ$  and  $\pm 15.1^\circ$  [5]. In this case, as the dimension of  $\mathbf{W}$  is  $4 \times 4$ , one can use the matrix inverse rather than the pseudo-inverse.

These results can be visually presented, as shown in the left plot of Fig. 1. The curves plot the values in the last three elements of  $\mathbf{W}_k$  as the compensator is rotated continuously over a full  $180^\circ$  rotation, and represent all the accessible states of the system. By connecting the four points when  $\theta$  is equal to  $\pm 51.7^\circ$  and  $\pm 15.1^\circ$  when a  $132^\circ$  retarder is used, the tetrahedron of maximum area is drawn. For  $N > 4$ , the  $132^\circ$  linear retarder also ensures a polyhedron of maximum volume [13]. Since the volume of a tetrahedron is one-sixth the determinant of the matrix containing its vertices, if we want to maximize the determinant to optimize our setup, we need to maximize the polyhedron volume as well [12,15].

If a second identical linear retarder is added to our system,  $\mathbf{S}_{\text{out}}$  changes to

$$\mathbf{S}_{\text{out}} = \mathbf{P}_1 \mathbf{R}(-\theta) \mathbf{M}_{LR} \mathbf{R}(-\phi) \mathbf{M}_{LR} \mathbf{R}(\phi) \mathbf{R}(\theta) \mathbf{S}_{\text{in}}, \quad (7)$$

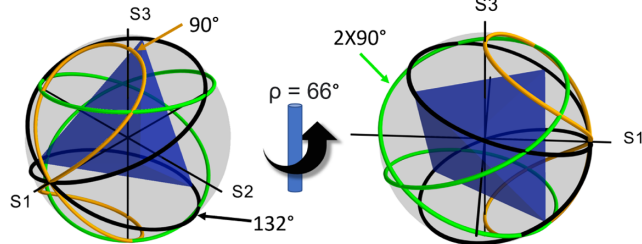


**Fig. 1.** Plot of the last three components of  $\mathbf{W}_k$  in Eq. (4) on the surface of a Poincaré sphere. In the left plot, the vertices of a tetrahedron of maximum volume are touching the  $132^\circ$  retarder system (black), while the  $90^\circ$  one (orange) does not access these points and is therefore less tolerant to noise. Upon rotating the sphere round  $S_3$ , the  $\mathbf{W}$  matrix for our system with two  $90^\circ$  retarders (green) is seen to be identical to the optimal  $132^\circ$  configuration.

where  $\phi$  is a relative angle between the two compensators. When  $\phi$  is not a multiple of  $90^\circ$ , the two compensators form an elliptical retarder,  $\mathbf{M}_E$ :

$$\mathbf{M}_E = \mathbf{M}_{LR} \mathbf{R}(-\phi) \mathbf{M}_{LR} \mathbf{R}(\phi). \quad (8)$$

Since any unitary element can be written as a product of a linear retarder followed by a circular retarder [16], we shall decompose the elliptical retarder as

$$\mathbf{M}_E = \mathbf{M}'_{LR} \mathbf{M}_{CR}, \quad (9)$$

where each component can be determined from

$$\mathbf{M}_{CR} = \mathbf{R}(\rho), \quad (10a)$$

$$\mathbf{M}'_{LR} = \mathbf{M}_E \mathbf{R}(\rho)^{-1} = \mathbf{M}_{LR} \mathbf{R}(-\phi) \mathbf{M}_{LR} \mathbf{R}(\phi) \mathbf{R}(\rho)^{-1} \quad (10b)$$

with

$$\rho = \frac{1}{2} \arctan \frac{M_{E12} - M_{E21}}{M_{E11} + M_{E22}}, \quad (11)$$

where  $M_{Eij}$  with  $i, j = 0, \dots, 3$  indicates the elements of  $\mathbf{M}_E$ . Equation (7) can thus be rewritten as

$$\mathbf{S}_{\text{out}} = \mathbf{P}_1 \mathbf{R}(-\theta) \mathbf{M}'_{LR} \mathbf{R}(\theta) \mathbf{R}(\rho) \mathbf{S}_{\text{in}}, \quad (12)$$

where  $\mathbf{M}'_{LR}$  is the linear retarder term of the elliptical retarder, and  $\mathbf{R}(\rho)$  is a rotation matrix representing the circular retarder. By setting an appropriate offset angle  $\phi$  between both linear retarders, the retardance of  $\mathbf{M}'_{LR}$  [Eq. (10b)] can be adjusted to a desired value. The linear retardance ( $LR'$ ) of  $\mathbf{M}'_{LR}$  is given by

$$\cos LR' = 0.25(3 + \cos(2LR) + T - 2 \cos(2\phi) \sin^2(LR)) - 1, \quad (13)$$

where  $T = \sqrt{\cos(2\phi) - 2 \cos^2(\phi) \cos(2LR) - 3}$ , and  $LR$  is the linear retardance of  $\mathbf{M}_{LR}$ . For a given value of  $LR$  between  $66^\circ$  and  $114^\circ$ , this equation can be solved numerically to find the angle  $\phi$  that creates the optimal  $LR' = 132^\circ$ .

For two  $90^\circ$  QWP retarders, the optimal relative offset  $\phi$  between the retarders was found to be  $24^\circ$ . At this angle, the linear retardance is  $132^\circ$ , while the optical rotation ( $\rho$ ) by Eq. (11) is  $66^\circ$ . In Fig. 1, this system can be seen to produce an equivalent trajectory on the Poincaré sphere as a single linear retarder with the optimal  $132^\circ$  retardance, since the green and the black curves trace the same paths along different parts of the sphere. The elliptical retarder we have described is therefore also capable of containing a polyhedron of maximal volume (for any  $N \geq 4$ ), and achieving an optimal conditioning of  $\mathbf{W}$ .

However, the ideal  $\theta$  angles  $\pm 51.7^\circ$  and  $\pm 15.1^\circ$  are not directly compatible with this system. The reason for this is that the effective linear retarder  $\mathbf{M}'_{LR}$  in Eq. (12) has a different azimuth angle than the original linear retarder  $\mathbf{M}_{LR}$  in Eq. (1), but this change of the azimuth can be easily determined as angular offset  $\Delta$ , which is therefore given as

$$\Delta = \frac{1}{2} \arctan \frac{M'_{LR13} - M'_{LR31}}{M'_{LR32} - M'_{LR23}}. \quad (14)$$

In the case of a dual QWP elliptical retarder,  $\Delta = -45^\circ$ , and the optimal angles are therefore  $[\pm 51.7^\circ, \pm 15.1^\circ] - 45^\circ = [6.7^\circ, -29.9^\circ, -60.1^\circ, -96.7^\circ]$ . If more than  $N = 4$  measurements are performed, the optimal angles found in previous

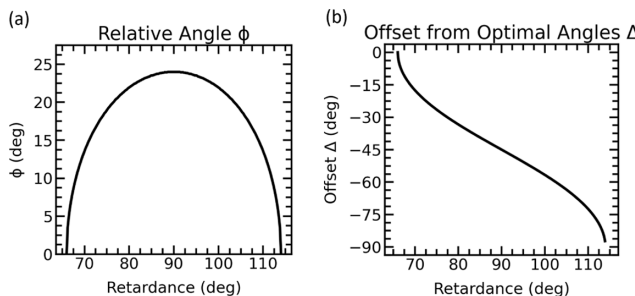


**Fig. 2.** Settings required to optimize the setup depending on compensator retardance. (a) The second retarder is placed at an angle  $\phi$  from the first retarder. Then, using the values in (b), the couple is rotated to the optimal angles for a  $132^\circ$  retarder setup, plus an offset  $\Delta$ .

studies (such as for  $N = 8$  measurements in [13]) can still be used by adding  $\Delta$  as a constant offset, achieving the same conditioning. If a retarder other than a QWP is used, the solutions to Eqs. (13) and (14) for all possible retardances can be seen in Fig. 2, for reference.

Since the elliptical retarder analysis works for any pair of retarders with  $\delta$  ranging from  $66^\circ$  to  $114^\circ$ , a spectroscopic polarimeter can also be designed using a film compensator. For example, if a Thorlabs WPQ10E-633 nm polymer zero-order quarter-wave plate is used, its retardance is around  $70^\circ$  at 750 nm, and  $110^\circ$  at 500 nm, with a linear relationship between retardance and wavelength at all values in between. Using a single setup, polarimetric measurements could therefore be taken at several wavelengths using this off-the-shelf non-achromatic wave plate within a spectral range of more than  $\pm 100$  nm by calculating the expected retardance of the wave-plate, and then using Eqs. (13) and (14) to adjust the relative angle  $\phi$  between retarders and the angular offset  $\Delta$ . The spectroscopic performance could be further improved by combining these results with genetic algorithm optimization methods capable of considering more general combinations involving a larger number of retarders with different retardances [17].

Additionally, we demonstrated the resilience to misalignment of the two compensators; Fig. 3 shows the effect of misaligning either the retarder group or only the second retarder by an angle  $\beta$ . Although the alignment of the relative angle  $\phi$  is more critical than the group angle  $\theta$ , the change in the value of the determinant of  $\mathbf{W}$  is still small, and even large misalignment values of  $\pm 5^\circ$  still achieve acceptable performance.

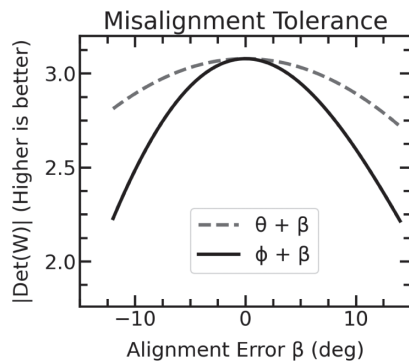


**Fig. 3.** Effect of misaligning either  $\phi$  or  $\theta$  on the determinant of  $\mathbf{W}$ . A misalignment of  $5^\circ$  on  $\phi$  causes less than a 10% decrease in the determinant.

**Table 1.** Performance Metrics of Four Example Stokes Polarimeters Using Different Linear Retarders ( $30^\circ$ ,  $90^\circ$ , and  $132^\circ$ ) or One Elliptical Retarder ( $2 \times 90^\circ$ )

Retardance	$\det(\mathbf{W})$	$\text{cond}(\mathbf{W})$	$\text{tr}([\mathbf{W}^T \mathbf{W}]^{-1})$
$30^\circ$	0.01	39.8	332.0
$90^\circ$	1.5	3.4	5.2
$132^\circ$	3.1	1.73	2.5
$2 \times 90^\circ, \phi = 24^\circ$	3.1	1.73	2.5

To validate the performance of the setup against noise, the equally weighted variance (EWV) metric is used, which gives an approximation of the variances of the Stokes vector estimate obtained from Eq. (5) [14]. We compute the EWV as the trace of  $(\mathbf{W}^T \mathbf{W})^{-1}$ , while setting  $\sigma^2 = 1$ , with the results shown in Table 1. It is clear that when a  $30^\circ$  retarder is used, the EWV has a large value, and the estimate of the Stokes vector will therefore have large variations. Both the optimal  $132^\circ$  retarder and our double  $90^\circ$  retarder setups achieve identical EWV values, and therefore have equal performance.

The performance of our setup and the effect of optimizing the metrics in Table 1 can also be represented visually. To do this, we divided a test image into four sections, each with a different Stokes vector (corresponding to vertical, left-handed circular and  $45^\circ$  polarizations, and to unpolarized light). The first component of Stokes vector is equal to the intensity of the image [Fig. 4(a)]. After multiplying each pixel by the matrix  $\mathbf{W}$ , the simulated intensity images can be seen in Fig. 4(b).

Upon multiplying the output intensity images by  $\mathbf{W}^+$ , the original image is recovered in the  $S_0$  measurement, while the polarization states at the different quadrants are also recovered, as seen in Fig. 4(c). When Gaussian noise is added to each of the four measured intensity images, the polarimeter is no longer able to fully recover the input image [Fig. 4(d)]. When a single  $30^\circ$  retarder with a large EWV of 332.0 is used, the estimated Stokes vector after adding the noise is seen to have large variations, and the sample image is not recovered. When the retarder is changed to a single  $90^\circ$  one, the EWV decreases to 5.2, and the system is clearly less affected by the noise with smaller variations around the expected Stokes vector estimate.

Finally, when we compare an optimal  $132^\circ$  system with the one using two  $90^\circ$  retarders with a  $\phi = 24^\circ$  relative angle between them, both systems have an EWV of 2.5, and the images appear identical. To quantify this, the root mean square (RMS) difference can be measured between each pixel of the input image and the output  $S_0$  image. When no noise is added to the system, the RMS difference is 0, while for the noisy image using a single  $90^\circ$  retarder, the RMS difference increases to 38.1. Both setups using either the  $132^\circ$  retarder or our elliptical retarder design achieve exactly the same RMS difference of 25.0. Therefore, the expected result that both systems are equivalently noise tolerant has been validated.

In summary, we have demonstrated the equivalency of a polarimeter using an elliptical retarder to the traditionally optimal design using a  $132^\circ$  retarder. This allows for much more readily available compensators to be used to build a setup quickly and inexpensively. In addition, these retarders are particularly well suited for imaging applications, especially when using large film compensators offering a wide FOV. To implement this design, one needs to find the required angle  $\phi$  between the retarders using Eq. (13), and then calculate the required

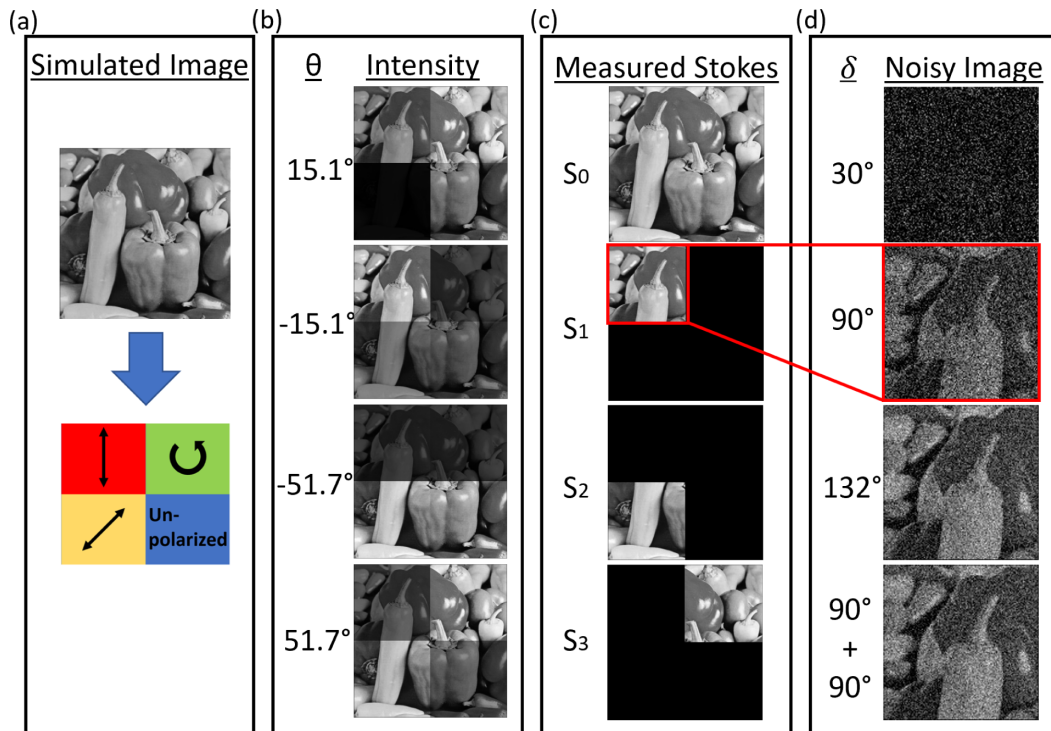


**Fig. 4.** (a) A test image is divided into four sections showing different polarizations, with the Stokes parameter  $S_0$  equaling the intensity at each pixel. (b) The simulated measured intensities by the setup are a series of  $N = 4$  images multiplied by  $\mathbf{W}_k$  at the angle  $\theta_k$ . (c) When no noise is added to the system, the original image is recovered in the  $S_0$  component perfectly, regardless of compensator retardance, and each of the polarization states are also recovered in other images. (d) After applying Gaussian noise to the four intensity images, the choice of compensator retardance changes the output image. Using a 30° retarder, almost no information on the input polarization states is visible. A 90° retarder achieves better performance, while both the single 132° retarder and our elliptical retarder design based on two QWPs achieve identical results.

offset found by Eq. (14) to add to the optimal angles found for a single retarder setup. Since these systems are equivalent, the results of these equations can be used directly for more than  $N = 4$  measurements, or more complex systems such as full Mueller matrix polarimeters by adding  $\phi$  and  $\Delta$  to both the polarization state generator and analyzer.

**Funding.** Ministerio de Ciencia Innovación y Universidades (RTI2018-098410-J-I00, RYC2018-024997-I, MCIU/AEI/FEDER, UE).

**Disclosures.** The authors declare no conflicts of interest.

**Data Availability.** Data underlying the results presented in this paper are not publicly available at this time but may be obtained from the authors upon reasonable request.

## REFERENCES

1. T. Novikova, A. Pierangelo, A. D. Martino, A. Benali, and P. Validire, *Opt. Photon. News* **23**, 26 (2012).
2. D. B. Murphy, *Polarization Microscopy* (John Wiley and Sons, 2012), pp. 153–171.
3. R. A. Chipman, *Handb. Opt.* **2**, 22.1 (1994).
4. O. Arteaga, M. Baldrís, J. Antó, A. Canillas, E. Pascual, and E. Bertran, *Appl. Opt.* **53**, 2236 (2014).
5. D. S. Sabatke, M. R. Descour, E. L. Dereniak, W. C. Sweatt, S. A. Kemme, and G. S. Phipps, *Opt. Lett.* **25**, 802 (2000).
6. F. Stabo-Eeg, M. Kildemo, E. Garcia-Caurel, and M. Lindgren, *J. Mod. Opt.* **55**, 2203 (2008).
7. S. Bian, C. Cui, and O. Arteaga, *Appl. Opt.* **60**, 4964 (2021).
8. X. Li, H. Hu, F. Goudail, and T. Liu, *Opt. Express* **27**, 31261 (2019).
9. S. G. Reddy, S. Prabhakar, A. Aadhi, A. Kumar, M. Shah, R. P. Singh, and R. Simon, *J. Opt. Soc. Am. A* **31**, 610 (2014).
10. S. G. Reddy, S. Prabhakar, P. Chithrabhanu, R. P. Singh, and R. Simon, *Appl. Opt.* **55**, B14 (2016).
11. R. Bettegowda, *Opt. Eng.* **56**, 034110 (2016).
12. K. Twietmeyer and R. Chipman, *Opt. Express* **16**, 11589 (2008).
13. J. S. Tyo, *Appl. Opt.* **41**, 619 (2002).
14. M. R. Foreman and F. Goudail, *Opt. Eng.* **58**, 082410 (2019).
15. R. M. A. Azzam, I. M. Elminyawi, and A. M. El-Saba, *J. Opt. Soc. Am. A* **5**, 681 (1988).
16. H. Hurwitz and R. C. Jones, *J. Opt. Soc. Am.* **31**, 493 (1941).
17. P. A. Letnes, I. S. Nerbø, L. M. S. Aas, P. G. Ellingsen, and M. Kildemo, *Opt. Express* **18**, 23095 (2010).